AD NUMBER
AD870792
LIMITATION CHANGES

TO:

Approved for public release; distribution is unlimited.

FROM:

Distribution authorized to U.S. Gov't. agencies and their contractors; Critical Technology; APR 1970. Other requests shall be referred to Air Force Weapons Laboratory, Kirtland AFB, NM 87117. This document contains export-controlled technical data.

AUTHORITY

AFWL ltr, 30 Nov 1971

AFWL-TR-69-154

AD870792

INVESTIGATION OF DYNAMIC MECHANICAL
STRESS WITH PHOTOELASTIC TECHNIQUES

V. R. Honnold   C. C. Berggren

W. M. Peffley

Hughes Aircraft Company
Fullerton, California 92634
Contract No. F29601-69-C-0095

TECHNICAL REPORT NO. AFWL-TR-69-154

April 1970

AIR FORCE WEAPONS LABORATORY
Air Force Systems Command
Kirtland Air Force Base
New Mexico

DDC
RECEIVED
JUN 24 1970
C

INVESTIGATION OF DYNAMIC MECHANICAL
STRESS WITH PHOTOELASTIC TECHNIQUES

V. R. Honnold   C. C. Berggren

W. M. Peffley

Hughes Aircraft Company

TECHNICAL REPORT NO. AFWL-TR-69-154

AFWL-TR-69-154

AIR FORCE WEAPONS LABORATORY
Air Force Systems Command
Kirtland Air Force Base
New Mexico

FOREWORD

This report was prepared by the Hughes Aircraft Company, Fullerton, California, under Contract No. F29601-69-C-0095. The research was performed under Program Element 62301D, Project 0251, Work Unit 008, and was funded by the Advanced Research Projects Agency (ARPA) under ARPA Order No. 251.

Inclusive dates of research were 1 April 1969 through 3 September 1969. This report was submitted 19 March 1970 by the Air Force Weapons Laboratory Project Officer, Lt Ralph S. Gross (WLTA).

Information in this report is embargoed under the Department of State ITIARs. This report may be released to foreign governments by departments or agencies of the U.S. Government subject to approval of AFWL (WLTA).

The authors would like to acknowledge the guidance and support provided throughout the program by Capt Daniel N. Payton III, and Lt Ralph S. Gross (WLTA) and the spirit of cooperation evidenced at all times by Mr. Robert Teng of McDonnell Douglas Astronautics Company and Dr. Howard Kratz of Gulf General Atomic during the performance of the contract. Appreciation is also extended to Capt David C. Straw of the AFWL TREE facility for his help on the mock-up tests.

This technical report has been reviewed and is approved.

RALPH S. GROSS
Lt, USAF
Project Officer

ROBERT H. HENSCHEID
Capt, USAF
Chief, Advanced Concepts Branch

CARL B. HILLAND
Lt Col, USAF
Chief, Technology Division

AFWL-TR-69-154

ABSTRACT

(Distribution Limitation Statement No. 2)

The technique of dynamic photoelasticity has been applied to a
study of hypervelocity impact phenomena. The target consisted of a
cadmium front plate, followed either by a void or a foam filled
space, and a rear plate of steel or aluminum. Two series of tests
were carried out. The first, employing a Plexiglas rod, acting as a
Hopkinson pressure bar in a transmission polariscope arrangement,
sensed the pressure time history resulting from debris stagnation
in the second plate. In the second series, the rear plate was pro-
vided with a photoelastic coating as part of a reflection polariscope.
Dynamic stress patterns, produced by a debris impact, were photographed
as they developed in time and provided a whole field view of the
nature of the pattern.

The experimental results indicate that Plexiglas can be used
successfully as a pressure bar for dynamic stress measurements in
the range of several kilobars. Analysis of dynamic plate motion
indicates the presence of elastic extensional waves and shows that
second plate deformation and rupture are accompanied by elastic
effects.

CONTENTS

PRECEDING PAGE BLANK

ILLUSTRATIONS

TABLES

SECTION I

INTRODUCTION

The study of hypervelocity impact is particularly challenging in the instrumentation requirements. This results both from the diversity of the material behavior and in the dynamic ranges involved. Two distinct aspects of the phenomena can be singled out for study. The first concerns the nature of the initial impact of the hypervelocity projectile, the production of a debris cloud and its subsequent behavior, and the second, the dynamic response of a second plate to the impulsive load provided by the debris stagnation pressure.

The report covers an investigation of the techniques of dynamic photoelasticity as applied to hypervelocity impact. Two different photo-elastic methods are utilized. In the first, a transmission polariscope is used to sense the debris stagnation pressure time history and represents a new version of the Hopkinson pressure bar that uses optical rather than electrical sensing. The second method studies the dynamic response of the second plate with a photoelastic coating and a reflection polariscope together with a high-speed framing camera. This technique provides a whole field view of the dynamic stress pattern, occurring in the plane of the plate, as it develops in time following impact of the debris cloud. The coating method is unique in providing a direct means of observing extensional and shear waves in the plate.

The report consists of three major sections. The first outlines the pertinent photoelastic equations, and covers dispersive effects that are important in analyzing the debris impact pressure time history. The second section covers the details of the experimental procedure, material selections, and sample preparations. A mock-up of the plate response experiment with the reflection polariscope was carried out at the AFWL Flash X-Ray Facility. This is covered in the third section together with a discussion and interpretation of the experimental results.

1

SECTION II

PHOTOELASTIC THEORY

1.   STRESS-WAVE PROPAGATION AND PRESSURE-TIME MEASUREMENTS

The present investigation utilizes the technique of photoelasticity
in the analysis of hypervelocity impact phenomena. In the experiments,
a dynamic stress pattern occurs in stress-birefringent material, in
the form of a coating or rod, and is detected with an appropriate form
of polariscope. In either case, because of the impulsive nature of
the loading, a wave motion of the medium can be expected and it is
necessary to consider certain aspects of wave propagation in inter-
preting the data.

The use of a rod or bar to sense impact time-history originated
with Hopkinson[1] who studied the nature of the pressure-time relations
when an explosive was detonated against or when a projectile impacted
a hard surface. Davies[2] developed an electrical version of Hopkinson's
pressure-bar and carried out a detailed analysis of the various correction
factors that need to be considered as a result of lateral inertia effects
and the finite length of the bar.

The present method of utilizing a rod of optically transparent
material to sense the stagnation-pressure time-history of debris
generated by hypervelocity impact can be based on the concept of the
Hopkinson pressure bar. The present scheme differs from those used by
Davies and Hopkinson, however, in that optical, rather than mechanical
or electrical sensing is utilized in detecting the propagation of the
stress wave. In the experiments of Davies, the displacement of the
end of the bar was made to vary the capacity of a condenser, one plate

2

of which is driven by the bar. The resulting electrical response was then recorded on an oscillograph. The pressure time history is obtained by differentiating the displacement in the expression,

$$p = \rho c_0 \, (du/dt) \tag{1}$$

where u is the displacement, and ρ and c_0 are, respectively, the density and longitudinal or bar wave velocity of the medium, $(E/\rho)^{1/2}$. In the present experiments, the pressure in Equation 1 is determined directly by detecting it passively as stress-induced birefringence in the sensing material itself.

Additional considerations are necessary, however, with respect to the accuracy of the "down stream" dynamic stress measurement in using it to determine the impact pressure-time history. These are the same as those considered by Davies, except that in the present case a rod with a rectangular rather than circular cross section is used. Estimates of accuracy in this connection can be based on studies by Morse and Davies. These will now be considered in more detail below.

The term configurational dispersion was introduced by Morse[3] to describe the dispersive nature of the propagation of elastic waves in a bounded medium, in particular in bars of rectangular cross section. It was found by Morse that dispersive effects from this cause become important when the wave length approximates twice the length of the larger side. In the present experiments, the larger side of the rod was 3/8 in. or 0.952 cm. For a typical impact duration of 20 microseconds, the effective upper frequency limit is 2×10^4 Hz, leading

to a minimum wave length of 5 cm for a velocity of 2.67×10^5 cm/sec.
It can be concluded, then, that dispersion from this aspect of rod
configuration can be neglected.

A second type of configurational effect is that due to the
finite length of the bar, rather than to its cross section.
This has been discussed by Davies as follows.

If a bar of length L is subjected to a constant force P per unit
area starting at the zero of time at the end x = L (pressure end) in
a direction toward the origin x = o, the subsequent displacement at
a point x and at a time t is given by,

$$u(x,t) = Pt^2/2m + (2PL^2/\pi^2 c_o^2 m) \sum_{n=1}^{\infty} \left[(-1)^n/n^2 \right] \cos(n\pi x/L) \times \left[1-\cos(n\pi c_o t/L) \right] \quad (2)$$

where m is mass per unit cross sectional area of bar.
The first term in the above expression represents the displacement of
the bar as a whole resulting from the acceleration P/m due to the
force acting for the time, t. The infinite sum represents vibrations
of the bar that are superimposed on this translational motion.

Davies considers this problem together with effects due
to lateral inertia of a rod, governed by the equation

$$\frac{\partial^2 u}{\partial t^2} - \nu^2 k^2 \left(\frac{\partial^4 u}{\partial x^2 \partial t^2} \right) = c_o^2 \left(\frac{\partial^2 u}{\partial x^2} \right) \quad (3)$$

where ν is Poisson's ratio, k is radius of gyration of the cross section
of a bar about the axis, and c_o is the bar velocity $(E/\rho)^{1/2}$.

After an extensive analysis, Davies concludes that for a
step function of pressure applied at one end, the rise
time at the measuring end will depend upon Poisson's

ratio and the radius (for a circular cross section) and length of the
rod. For a typical case of a rod 1 in. in diameter and 2 feet 2 inches
long, the observed rise time as calculated by Davies is about 3 micro-
seconds. This latter number can be taken as representative for our case
of a rectangular bar; it means that the rise time for a step function
of pressure for the bar used in the present invesitgation is a few
microseconds at most.

2. MATERIAL DISPERSIVE EFFECTS

The propagation of mechanical waves in viscoelastic solids has
been discussed by Kolsky[4]. Dispersion for this class of materials
occurs because the phase velocity and attenuation increase with
increasing frequency.

Kolsky studied the propagation of short mechanical pulses along
rods of several types of plastics. The pulse was produced by the
detonation of small quantities of explosives at one end of a rod. A
condenser microphone at the other sensed the time-dependent displace-
ment. This is seen to be the Hopkinson bar technique applied to visco-
elastic materials and Kolsky's experimental results are pertinent to
the present investigation.

Basically, if the response of a material to sinusoidal stress
over a range of frequencies is known, the upper limit of which is
determined by the reciprocal of a stress pulse duration, then the time-
dependent behavior of a pulse shape can be determined as it propagates
along a rod of material.

For a plane sinusoidal stress wave traveling in a viscous material,
with the time dependence $\sigma_0 \cos \omega t$ at the origin, its amplitude at an

5

arbitrary position x will be given by $\sigma_0 \exp(-\alpha x) \cos \omega(t-x/c)$ where α is the attenuation constant of the material, and c is the propagation velocity of the wave. The constant α is related to a loss factor, tan δ, by the equation[5],

$$\alpha = (\omega/4\pi c) \times (\Delta w/w) = (\omega/2c) \tan \delta \qquad (4)$$

where $\Delta w/w$ is the fractional energy loss per cycle, under sinusoidal excitation at angular frequency, and δ is the angular phase lag between stress and strain at ω.

It was found empirically by Kolsky for three polymers, including polymethyl methacrylate (Plexiglas), that there was a similarity of form for a pulse as it was observed after traveling through various distances of material. That is, by a suitable extension of time scales and amplitudes, all pulse shapes were approximately the same.

Hunter[6] has discussed the pertinent equations for the present investigation. Consider a semi-infinite rod subjected to a time-dependent stress at the origin, x = o. If the stress is denoted by $\sigma(0,t)$, then the stress at a position, x, as a function of the time, t, will be given by the expression,

$$\sigma(x,t) = \int_{-\infty}^{+\infty} \sigma(o,t') \sigma_1(x, t-t')dt', \qquad (5)$$

where $\sigma_1(x,t)$ represents the response to an impulsive load $-P_0\delta(t)$ at the origin. It can be shown[6] that the impulsive response $\sigma_1(x,t)$ is given by the expression

$$\sigma_1(x,t) = (1/2\pi) \int_{-\infty}^{+\infty} e^{i\omega(t-x/c)} e^{-\alpha x} d\omega \qquad (6)$$

Now generally in a dispersive medium with loss the phase velocity c and attenuation α are functions of frequency. In the ideal case these

functions would be inserted in Equation 6 and the integration carried out. This would be a difficult task in this case and additionally the dependence of the phase velocity on frequency does not appear to have been determined. Therefore, an approximate procedure will be used that has been found to yield reasonably good results for pulse shapes produced in a selection of plastic rods including Plexiglas. The loading was provided by detonation of an explosive charge and was of a few microseconds duration. The approximations, following Hunter, are that the phase velocity is approximately constant with frequency,

$$c(\omega) \approx c_0 \tag{7}$$

and that the attenuation, α, is a linear function of angular frequency, ω,

$$\alpha(\omega) = k\,\omega, \tag{8}$$

where k is defined in terms of the loss tangent, $\tan \delta/2$, and the phase velocity, c_0, as follows,

$$k = (1/c_0) \tan (\delta/2) \tag{9}$$

These expressions are seen to be of the form given in Equation 4 above. With Equations 8 and 9, Equation 6 can be integrated directly to give,

$$\sigma(x,t) = \frac{kx/\pi}{k^2 x^2 + (t - x/c_0)^2} \tag{10}$$

With this explicit expression for the impulsive response of the rod, it is possible now to form an estimate of the degree of change in pulse shape that occurs between the pressure end at $x = o$ and the point

at which the measurements are made. In order to keep the calculations
in fairly simple form, the input stress will be assumed to be a linear
function of time to a time T at which the stress has an amplitude,
σ_o, which remains constant for $t > T$. The resulting response can then
be examined at the particular point at which observations were made.
The explicit expressions then are,

$$\sigma(o,t) = (\sigma_o/T)\,t, \quad 0 \leq t \leq T \tag{11}$$

$$\sigma = \sigma_o, \quad t > T \tag{12}$$

Equations 11 and 12, can be combined with Equation 9 and inserted in
Equation 5 for the response $\sigma(x,t)$. This gives

$$\sigma(x,t) = (\sigma_o/\pi T) \int_0^T \frac{kx\,t'\,dt'}{k^2x^2 + (t-t'-x/c_o)^2} +$$

$$(\sigma_o/\pi) \int_T^\infty \frac{dt'}{k^2x^2 + (t-t'-x/c_o)^2} \tag{13}$$

The integrations can be carried out and the result is plotted in
Figure 1 in the dimensionless time unit $(t-x/c_o)/kx$ where x is the
observation point. In the present case x is taken to be 12 cm. The
value of k is calculated in accordance with the values for Plexiglas
given by Kolsky, tan $(\delta/2) = 0.04$ and $c_o = 2.2 \times 10^5$ cm/sec. The time
T is taken as 10 µsec as a representative rise time. The original input
at $x = o$ is also shown superimposed and centered at the origin. While
rounding off of the input time history is apparent, the rise time and
amplitude are reproduced reasonably well. Bearing in mind that the actual
impulse is itself not as angular as the idealized form shown, it is con-
cluded that the measured response, as will be discussed below, should rep-
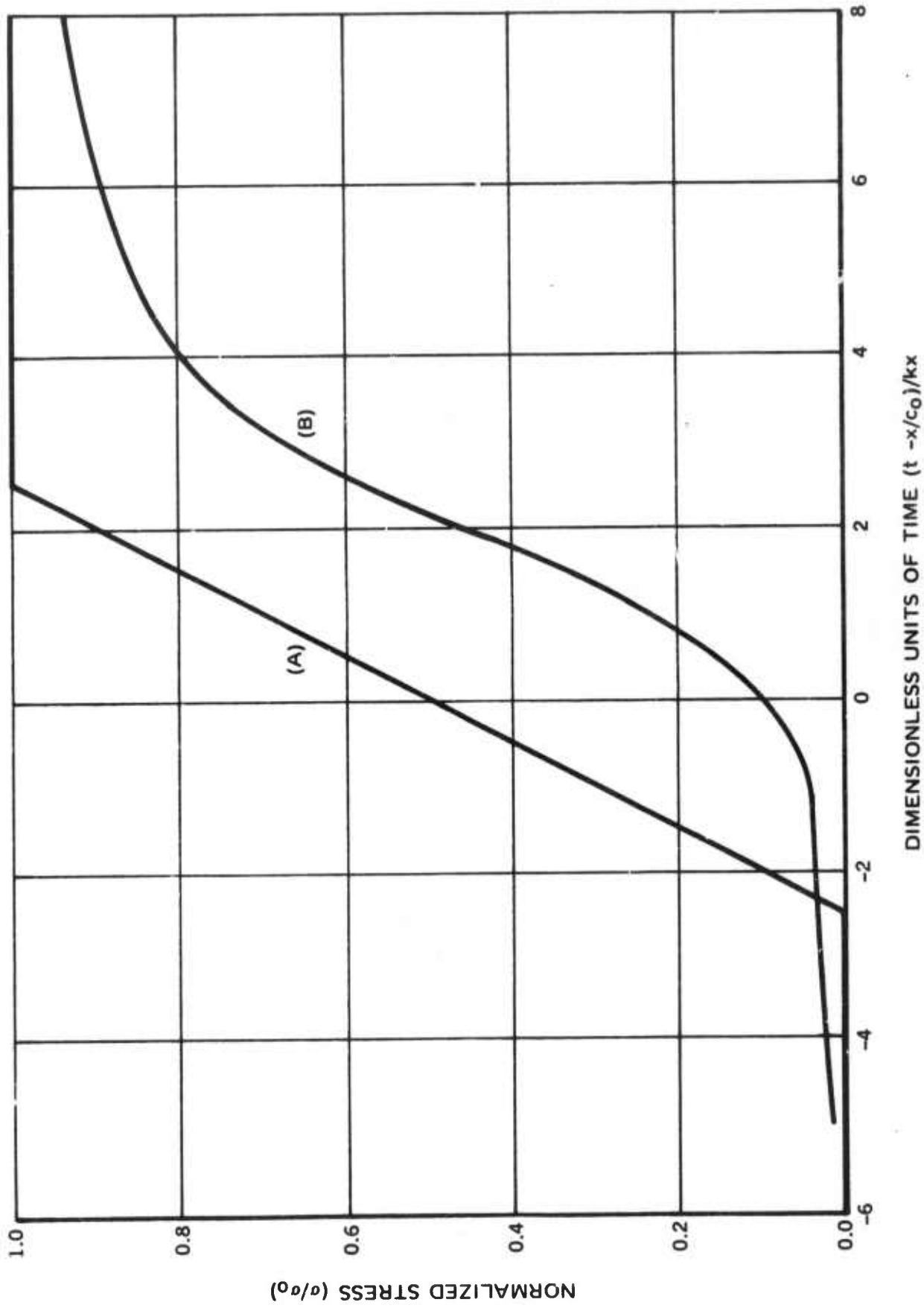resent the actual time history with an accuracy of approximately ten
percent.

Figure 1: Stress Time History

(A): Input stress time history at x = 0

(B): Stress time history at x = 12 cm
$k = 1.83 \times 10^{-8}$ sec/cm; $c_o = 2.2 \times 10^5$ cm/sec.

DIMENSIONLESS UNITS OF TIME $(t - x/c_o)/kx$

NORMALIZED STRESS (σ/σ_o)

3. PHOTOELASTICITY AND THE POLARISCOPE

Light entering an anisotropic medium is, in general, refracted into
two plane-polarized components traveling with different velocities. A
number of materials which are isotropic in a relaxed state exhibit such
behavior upon the application of stress. The relative path retardation
experienced by these components as they emerge from the sample is
directly proportional to the difference of the principal stresses in
the material. These phenomena, the photoelastic effect, which permit
an optical determination of the stress present in a transparent material,
and the optical instruments, known as polariscopes, which measure these
retardations, have been discussed by many authors[7]. Polariscopes are
used both to measure static stresses, and by employing suitably fast
detectors, to measure time-dependent transient stresses.

The intensity of light transmitted through a plane polariscope
which has the axis of the analyzer perpendicular to the axis of polar-
ization is

$$I = K \sin^2(2\alpha) \sin^2(\Delta/2) \tag{14}$$

where K is a proportionately constant, α the angle between the axis of
polarization of light incident upon the test sample and the direction
of one of the principal stresses and Δ, the retardation, is given by

$$\Delta = 2\pi d C \sigma / \lambda \tag{15}$$

C is the stress-optic coefficient, d the thickness of the sample, σ the
difference between the principal stresses in the plane normal to the
polariscope axis, and λ the wave-length of the light. Thus the inten-
sity of the light transmitted through the plane polariscope is deter-
mined not only by the difference in the magnitudes of the principal
stresses, but also by their direction.

The addition of quarter-wave plates to the plane polariscope results in a circular polariscope which eliminates the conflicting effects of stress directions. The circular polariscope is used both in open-field and closed-field configurations. In the open-field arrangement the maximum intensity of light is transmitted through the polariscope when the principal stress difference is zero.

The governing equation for the open-field circular polariscope is

$$I = I_o \cos^2 (\Delta/2) \tag{16}$$

where I_o represents the transmitted light intensity at zero stress difference. With the closed-field circular polariscope the intensity possesses a sine-squared dependence and is zero when the stress difference is zero.

SECTION III

EXPERIMENTAL PROCEDURE

1. CONFIGURATION OF THE DYNAMIC POLARISCOPE

The theory of operation of a circular polariscope is discussed at length in several excellent sources[8,9]. Essential elements consist of a light source, polarizing elements, a quarter-wave plate, a sample exhibiting stress birefringence, a second quarter-wave plate, an analyzer, and a recorder. Several investigations, notably Cole[10] and Flynn[11] have successfully applied this stress detection scheme to the dynamic response of plates and rods to mechanical impact.

The following two sections contain a description of the instrumentation of a stress coat polariscope and transmission polariscope. These were applied to an analysis of target plate response and debris stagnation pressure during hypervelocity impact tests at the McDonnell Douglas Astronautics Co. - Western Division light gas gun facility.

a. Reflection Polariscope

To apply the technique of stress birefringence to measure the stress distribution in the plane of the target plate involves the application of stress coat analysis. The stress coat is a layer of birefringent material bonded to a suitably polished surface of the target plate. The dynamic response of the plate is then observed via the transfer of stress to the coating material. Essential elements of this arrangement are shown in Figure 2 and are listed below.

- Xenon flash lamp-Operation* at peak output of approximately 400 megalumens with a flash duration of 40 microseconds.

* Beckman and Whitley Model 124
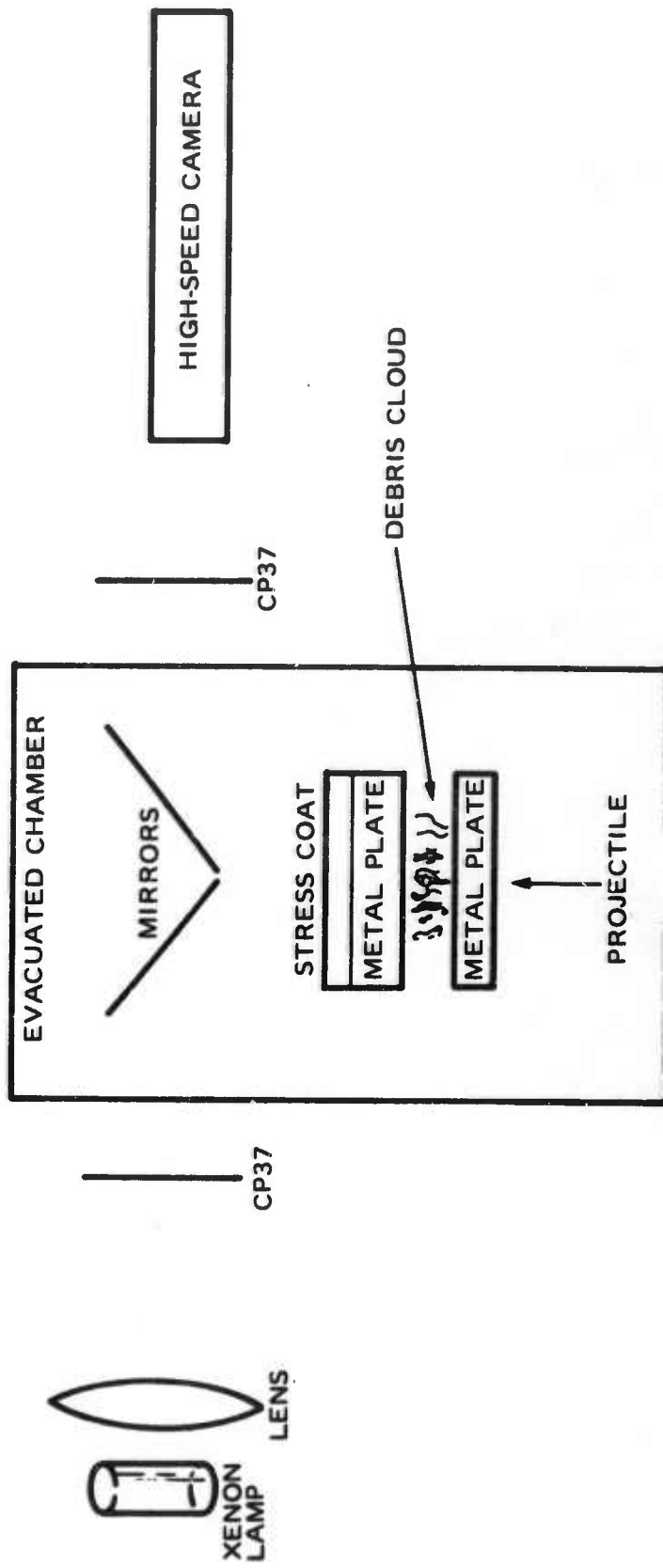
Figure 2. Reflection Polariscope

- Condensing lens - Glass, 8-inch diameter 36-cm focal length double convex lens. Placement with respect to flash lamp was set to focus all available light on the slit system of the high-speed camera.

- CP37* - Linear analyzer and quarter-wave plate fixed in an orientation to yield an open-field polariscope arrangement. Two used, one just outside each Plexiglas window on the impact chamber.

- Mirrors - Front surfaced mirrors of aluminum deposited on selected quarter-inch plate glass (maximum seven fringes per inch).

- Stress coat** - Polyster resin (see following section on materials selection rational).

- Target plate - 1/8-inch mild steel or 1100-0 Al, cloth-buffed to a bright shine. This plate is driven by debris from impact of a cadmium sphere on a front plate of 1/16-inch cadmium which is separated by 2-3/10 to 3-2/5 inches of void or foam from the target plate (see Table I for details of shot sequence).

- High-speed camera*** - Stress pattern was recorded on 35-mm film at an approximate speed of 10^6 frames/sec.

*   Polaroid Corporation CP 37
**   Homalite 100
***   Beckman and Whitley Model 330

Kodak 2484 film processed at an ASA speed of 2000 was used
in the high-speed camera. The exposure time was approximately
.33 μsec/frame and the field of view a 4 x 6 inch rectangle.

b. Transmission Polariscope

The polariscope was applied to a measurement of debris
stagnation pressure on a half-inch back plate through the use
of two Plexiglas probes. These probes were 1/16-inch-thick
Plexiglas cut to 3/8-inch-wide by 12-inch-long bars. An 11/16-
inch hole was drilled in the half-inch steel plate and the probes
inserted in pre-moulded forms of RTV-11 silastic rubber. Impact
of debris on the end of these rods resulted in stress waves
which were detected through modulation of the transmitted laser
beam approximately five inches from the front of the rod.

The essential elements of this polariscope arrangement are
shown in Figure 3.

- Laser* - He-Ne laser operated at the 6328 Å
  line. This laser emits a plane polarized,
  1/16-inch-diameter beam of approximately 20mW.

- a - Mica quarter-wave plates mounted in glass.

- b - Half-silvered beam-splitter mirror (55% trans-
  mission, 45% reflection).

* Spectra - Physics Model 124
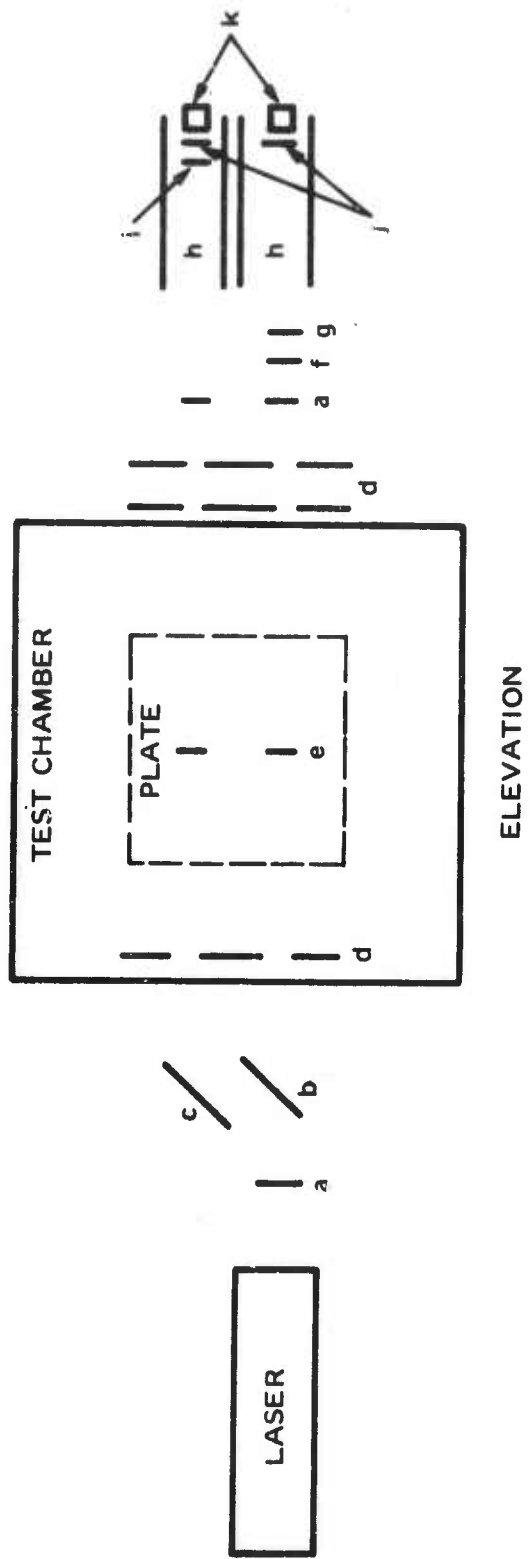
Figure 3. Transmission Polariscope

- c - Front surfaced mirror.

- d - Black-paper slit system, used to prevent the photodiodes from being exposed to the intense glow of the debris cloud.

- e - Plexiglas probes (see the following section for materials selection analysis).

- f - g - Combination of interference filter passing the 6328-Å-laser line and an infrared cut-off filter to suppress light transmitted in this region by the interference filter.

- h - Brass tubes to support the optical elements and provide additional light shielding.

- i - Wratten filter number 24 used to eliminate a portion of the impact flash.

- j - Polaroid analyzer sheets.

- k - PIN silicon photodiode*, used with 45 volts reverse bias and a 100-ohm load. These devices are capable of recording better than a 1/10 microsecond rise time.

* United Detector Technology Type 8LC

2. MATERIALS SELECTION AND PREPARATION

    a. Reflection Experiment (Plate Dynamic Response)

        Stresses in the plane of the plate were measured by a
    photoelastic coating technique. The stress coat material sel-
    ected for the reflection polariscope tests was Homalite 100, a
    polyester resin. Selection of this material was based on a
    search of the literature on stress coat materials with final
    evaluation at a mock-up test at the AFWL. Requirements for a
    useful material include transparency, ease of bonding to both
    steel and aluminum, uniformity of thickness and sufficient
    sensitivity to assure observable fringe patterns with a mini-
    mum of strength. The latter requirement is to insure the
    stress coat does not contribute to the stress pattern in the
    metal but simply acts as a sensor.

        Candidate materials selected for the mock-up test at the
    AFWL FXR facility included Hysol Corporation's RU-2085 and
    R9-2053 polyurethane resins and Homalite 100 polyester resin.
    These materials were obtained in the form of casting resins
    for this test. The polyurethane resins displayed sufficient
    bonding strength but became discolored and soft after several
    days. The Homalite 100 casting resin did not adhere well to
    the polished metal plates, however, its superior sensitivity
    (see the following section for test results) suggested the
    use of pre-cast Homalite 100 sheets. For the experiments at
    the hypervelocity impact range these pre-cast sheets were
    successfully bonded to the metal plates with an epoxy adhesive.*

* Homalite 1100 Epoxy Adhesive

b. Transmission Experiment (Debris Stagnation Time History)

Plexiglas was selected as the material for the measurements of debris stagnation pressure induced normal to the plane of the back plate. Among the necessary requirements for a satisfactory probe material were that it be transparent to the 6328-$\overset{o}{A}$-laser line, rigid, machineable, and not too brittle. A knowledge of the stress-optic coefficient and the stress-wave velocity was also required. Further, since the stress was monitored not directly at the back plate, but at a point several centimeters from the front of the probe, it was important that attenuation of the stress pulse by the probe be small.

Quartz and several alkali-halides were considered as probe materials but were rejected since, as crystals, they are each characterized by several stress-optic coefficients corresponding to different crystal orientations. Numerous glasses were considered and while their stress-optic coefficients were, in general, slightly less than the stress-optic coefficient of Plexiglas, the glasses were too brittle and susceptible to breakage.

Plexiglas is the most easily machined of the materials considered and values of its stress-optic coefficient and its longitudinal and shear stress wave velocities are known. A calculation of stress pulse propagation in Plexiglas, based upon frequency-dependent attenuation coefficient data, indicates that attenuation effects could be accurately determined. In this calculation Plexiglas was treated as an elastic material and dispersion effects were neglected. For example, the amplitude of a five-microsecond-wide rectangular-shaped stress pulse was found to be reduced by only ten percent after traveling ten centimeters through Plexiglas. It should be added that no serious drawbacks to the use of the Plexiglas probes were found as a result of their use in the present tests.

SECTION IV
EXPERIMENTAL RESULTS

The main experimental sequence consisted of two groups of four shots each. The first series included the reflection polariscope arrangement to monitor radial stress patterns in the second plate while the second series was the transmission polariscope technique to measure debris stagnation pressure. The shot configuration is presented in Table I.

TABLE I
SHOT CONFIGURATION

Shot Number	Material Configuration	Target Dimensions
5	Cd/Cd-V-Fe	1/(1/4-8-3/4)
7	Cd/Cd-V-Al	1/(1/4-12-3/4)
11	Cd/Cd-f-Fe	1/(1/4-8-3/4)
13	Cd/Cd-f-Al	1/(1/4-12-3/4)
22	Cd/Cd-V-Press	1/(1/4-8-Press)
23	Cd/Cd-V-Press	1/(1/4-12-Press)
24*	Cd/Cd-V-Press	1/(1/2-8-Press)
25	Cd/Cd-f-Press	1/(1/4-8-Press)
26	Cd/Cd-f-Press	1/(1/4-12-Press)

a. Cd/Cd-V-Cd means cadmium sphere onto cadmium front plate, a void, and a cadmium rear plate; f designates foam between the plates.

b. 1/(1/4-8-3/4) means that if the sphere has a diameter $\equiv$ 1, then the front plate has a thickness of 1/4, the spacing between the plates is 8, and the rear plate has a thickness of 3/4.

c. Foam density is 0.1 gm/cm^3.

d. Aluminum is 1100-0.

* Shot 24 was added when data on 22 was lost due to experimental problems.

1. STRESS COAT RESPONSE TO FLASH X RAY

The mock-up test at the AFWL was intended to provide a basis for selection between stress coat materials. The results, however, also indicate the great potential for this technique to analyze stress induced by electron energy deposition in structures.

The experimental arrangement is essentially that shown in Figure 2 with the substitution of a light source* and a TRW image converter camera**. The flash lamp was set for near normal incidence and two mirrors employed to allow removal of the film and electron optics from the radiation area.

One example of the data obtained is shown in Figure 4. In this experiment, a 1/16-in. steel plate was provided with a coating and exposed to the direct beam of a 2-MeV flash X ray, directed normal to the plate and on the side opposite to the coating. The response is shown with time proceeding downward from the top. Three frames are shown with the FXR pulse exposure occurring between the first and second frames. The time interval between the first two frames is two microseconds and between the second and third, five microseconds. The propagation of an axisymmetric wave outward is evident. The central dark spot that is unchanged with time is caused by a distorted region in the coating left by a preceeding exposure. The two dark rectangles at the bottom of each frame are markers spaced an inch apart to set the scale.

The production of the axisymmetric stress wave in this experiment parallels closely that observed in the impact experiment following impulsive loading from debris stagnation. Further discussion, accordingly, is deferred to Section IV below where the latter experiment is discussed in detail.

* GE FT220
** TRW Model 28B

AFWL-TR-69-154
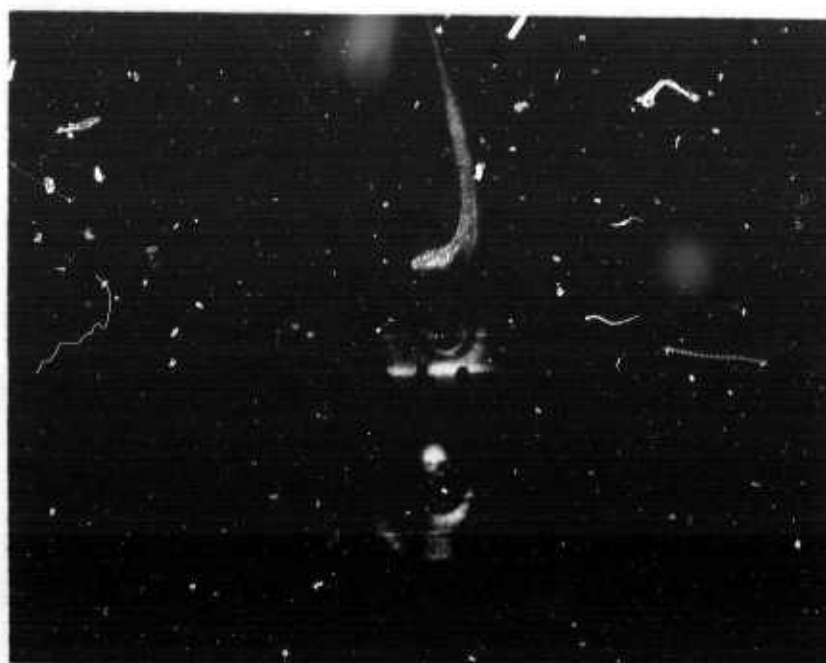
Figure 4. Dynamic Photoelasti Response Of A Steel Plate To A
Pulsed Electron Beam. 2 µsec Between Top Frame And
Center Frame. 5 µsec Between Center Frame And Lower
Frame. 0.5 µsec Exposure Time.

22

2. HYPERVELOCITY IMPACT TESTS

a. Transmission Polariscope Measurements

Stress measurements with the transmission polariscope were successfully performed on four hypervelocity shots (23, 24, 25, and 26). Shot 24 was not included in the planned series of transmission polariscope shots but was added when data was not obtained on shot 22. On shot 22, the stress-sensing photodiodes were driven off scale by a large "impact flash" of light resulting when the debris cloud impacted on the second plate. The diodes were consequently unable to monitor the passage of the stress pulse in the probe material. This impact flash problem, which appeared to be most serious with the void shots, was overcome by incorporating additional light shielding to form a collimated optical path and by the use of appropriate optical filters.

Pressures were measured at two points on each back plate, these points being centered one inch above and one inch below the center of the plate. Figure 5 depicts the plates, probe positions, and approximate impact locations for the four shots. The plates are shown as viewed from the rear of the evacuated chamber (See Figure 2) and the area of maximum impact pressure are shown as crosses.

Figures 6, 7, 8, and 9, show representative transmission polariscope responses to the stresses induced by the impacting debris clouds of shots 23, 24, and 25. The oscilloscope was triggered approximately 3 μsec after front plate impact. The time interval from the oscilloscope triggering to the onset of the stress pulse results primarily from the time required for the passage of the stress pulse along the Plexiglas probe to the laser beam position. The distances from the front face of the back plate to the laser beam probe position are given in Figures 8 and 9. This distance was 146 mm on shot 26 but was not recorded on shot 23. Also shown are the corresponding

AFWL-TR-69-154
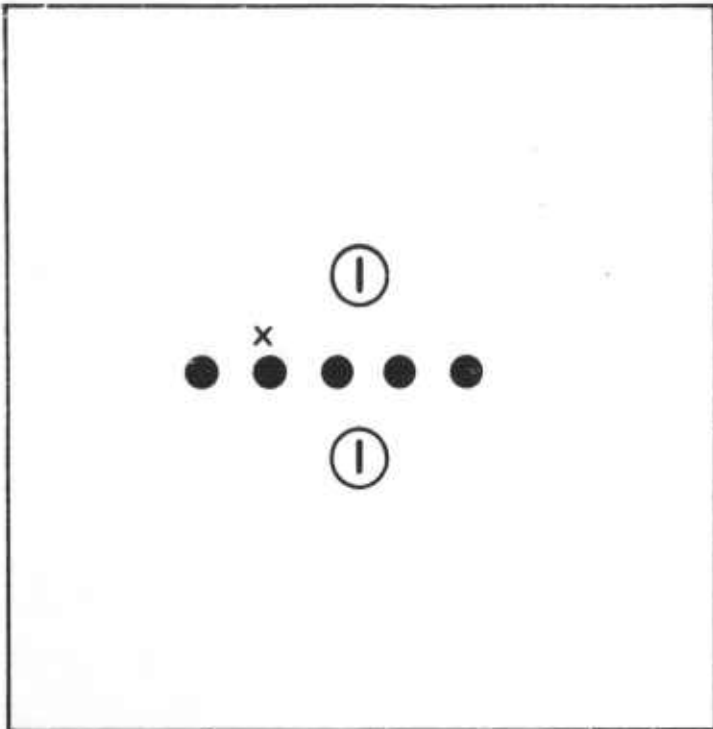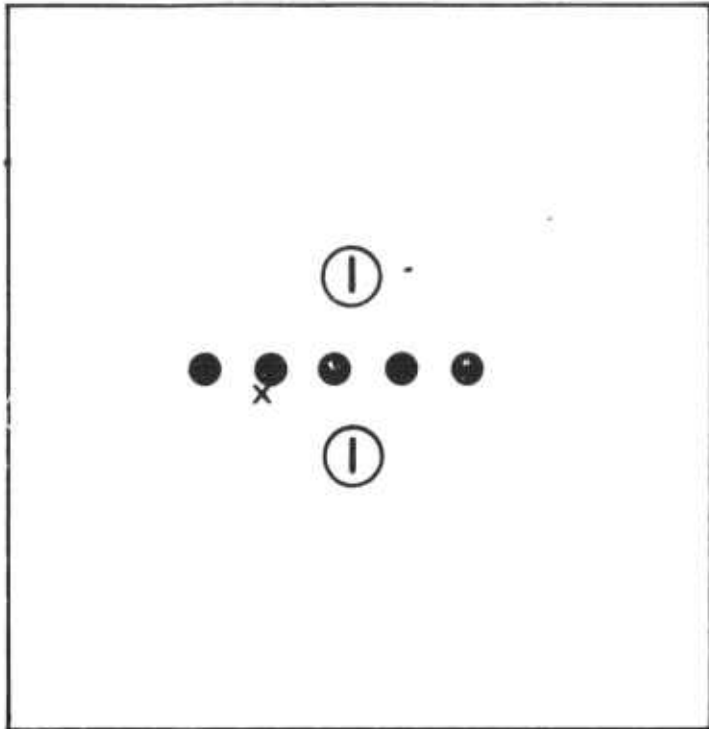
SHOT 23

SHOT 24

SHADED CIRCLES INDICATE POSITIONS OF GULF GENERAL ATOMIC STRESS PROBES
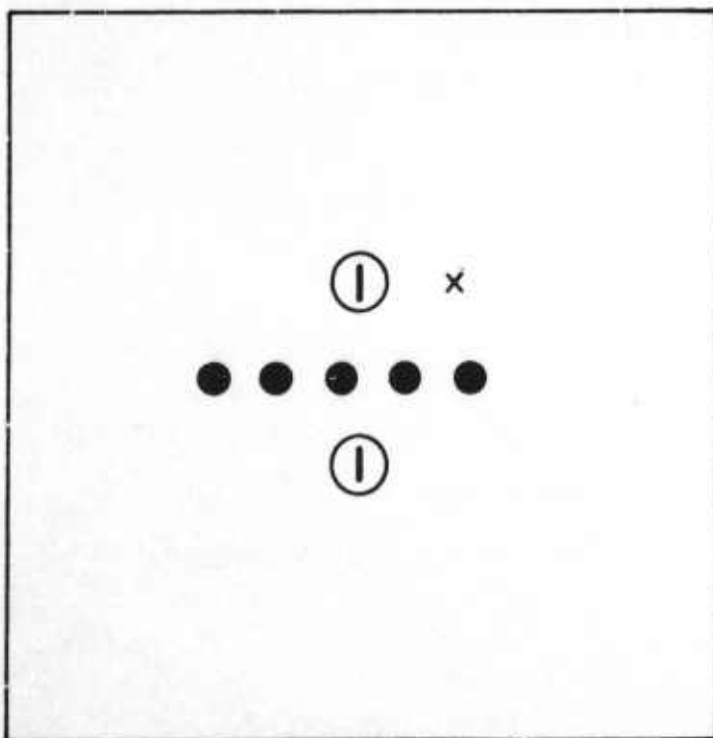
SHOT 25
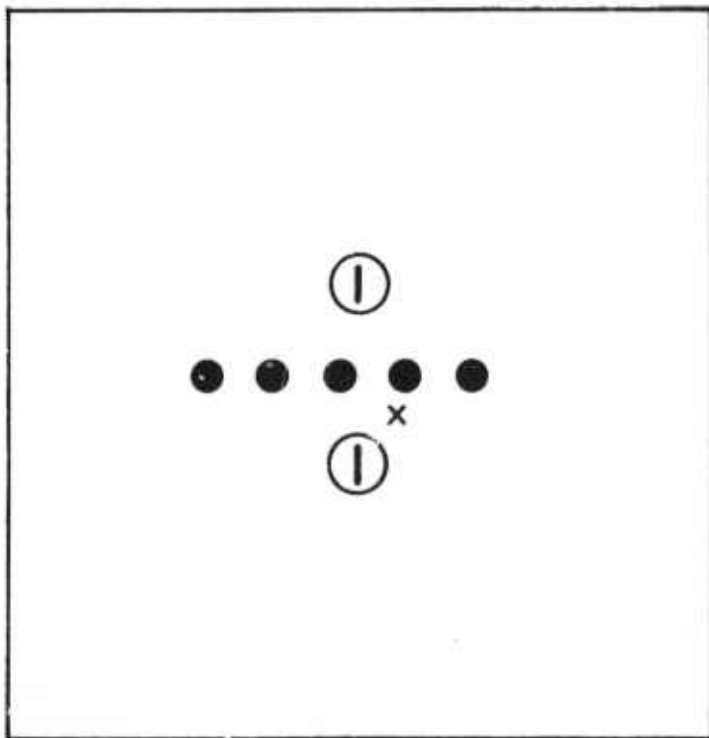
SHOT 26

Figure 5. Approximate Locations (Shown As Crosses) Of Maximum Impact Pressure
On Back Plates For Shots 23-26. Plexiglas Pressure Probes Are
Shown In Circles.

Polariscope Response To Induced Stress Pulse - Shot 23,
Upper Probe. Sweep Speeds: Upper Trace - 10 usec/Div.
Lower Trace (Delayed) - 5 μsec/Div.
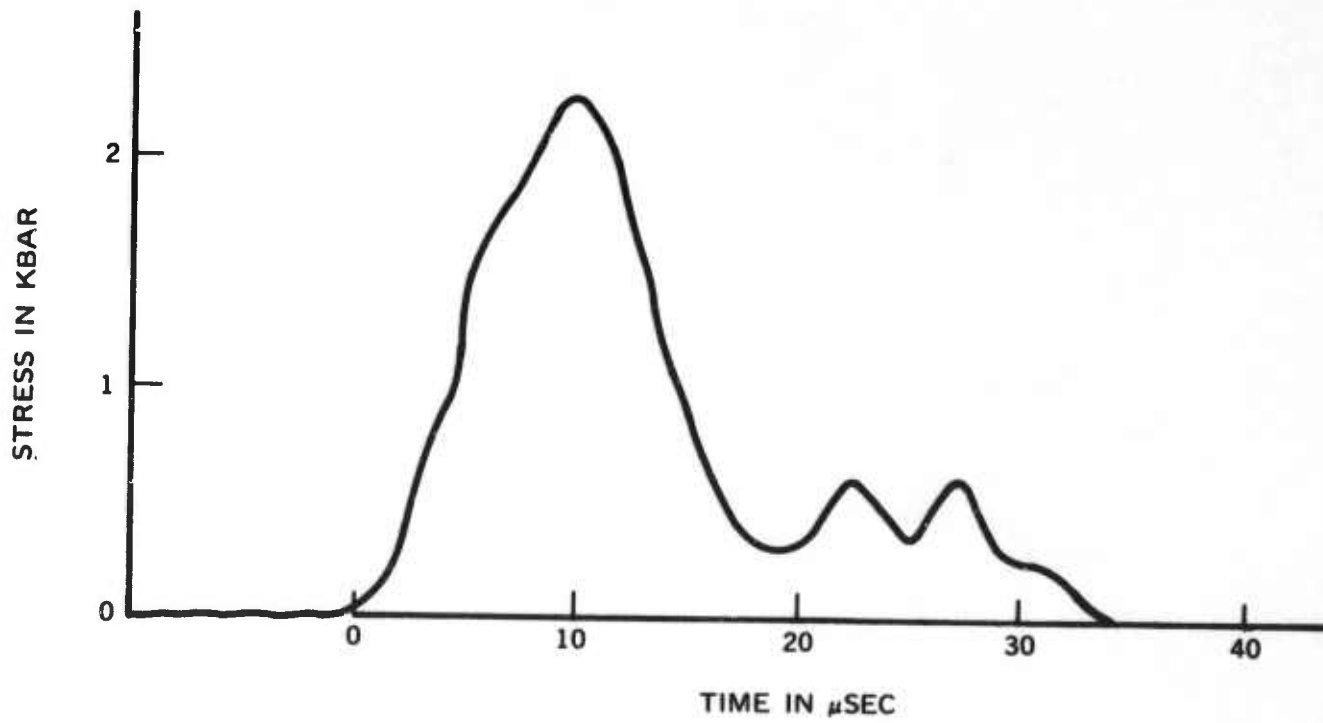
Figure 6. Stress Pulse Measured By Upper Probe - Shot 23
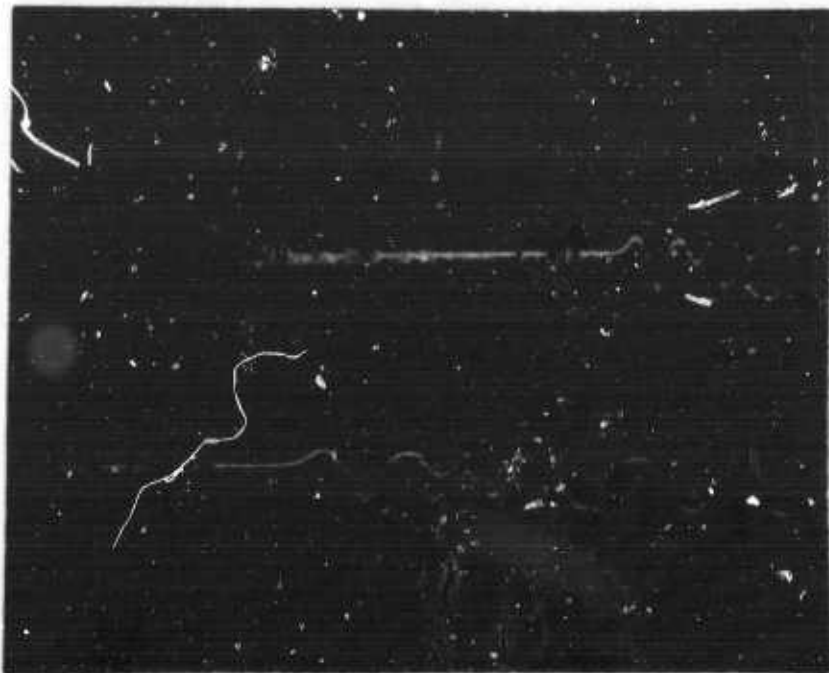
Polariscope Response To Induced Stress Pulse - Shot 23,
Lower Probe. Sweep Speeds: Upper Trace - 10 usec/Div.
Lower Trace (Delayed) - 5 usec/Div.

Figure 7. Stress Pulse Measured By Lower Probe - Shot 23

Polariscope Response To Induced Stress Pulse - Shot 24,
Upper Probe. Sweep Speed: 20 usec/Div.
Distance From Front Face Of Back Plate To Laser Beam Position = 146 mm

Figure 8. Stress Pulse Measured By Upper Probe - Shot 24

Polariscope Response To Induced Stress Pulse - Shot 25,
Upper Probe. Sweep Speeds: Upper Trace - 20 μsec/Div.
Lower Trace (Delayed) - 5 μsec/Div.
Distance From Front Face Of Back Plate To Laser Beam Position = 127 mm
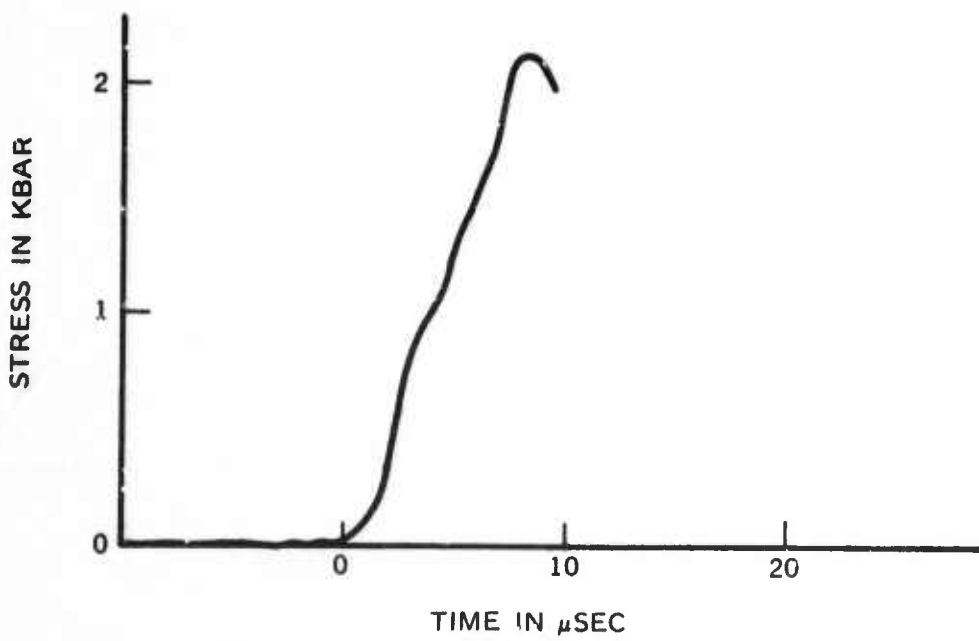
Figure 9. Stress Pulse Measured By Upper Probe - Shot 25

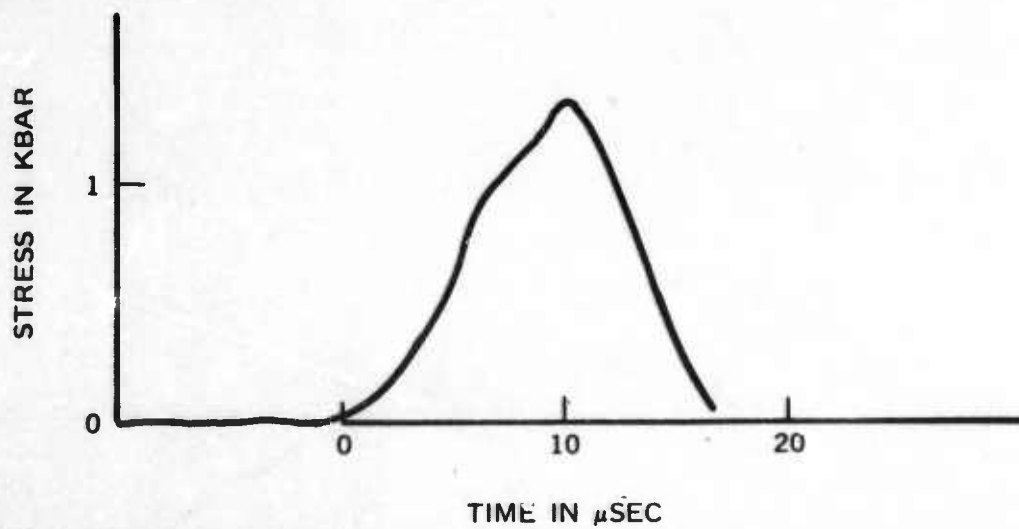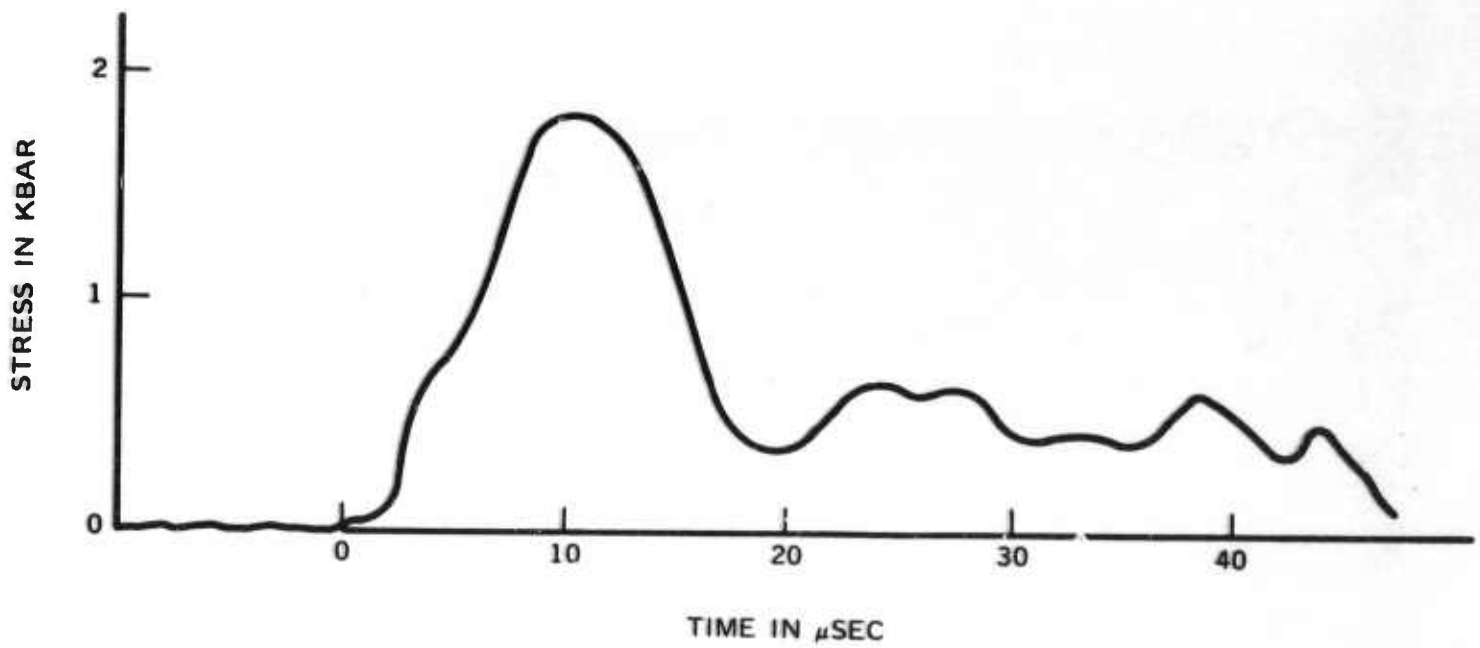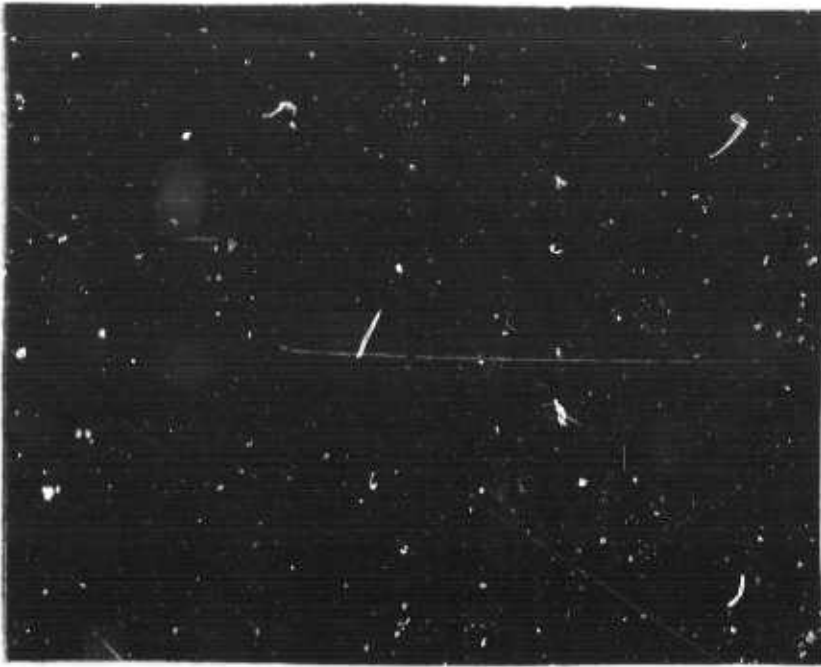time-dependent stress pulses, as determined by mapping the data
from the polariscope responses through Equation 16. Time is
measured from the arrival of the stress pulse at the laser beam
position. The polariscope was operated in an open configuration
so that decreases in the diode voltage correspond to decreases
in light intensity. The polariscope responses were recorded at
two sweep speeds. The lower sweep for shot 24 - upper probe did
not trigger and this trace was not recorded. However, the
complete data were recorded on the upper trace.

The lower trace of Figure 6 shows the response of the
polariscope to a stress pulse registering a peak pressure of
2.26 kbar. The data were taken with the upper probe on shot
23. The sweep speed is 5 μsec/div. The peak pressure occurs
about 9 μsec after the leading edge of the stress pulse arrives
at the detector. Symmetry about this peak point is evident
in the oscilloscope photograph except for oscillations which
occur in the tail of the decreasing stress, beginning about
10 μsec after the peak of the pulse.

The lower probe on shot 23 recorded the response shown
in Figure 7. The measured peak pressure of 1.36 kbar was
found to occur about 10 μsec after the arrival of the stress
pulse at the lower beam position.

Figures 8 and 9 show the polariscope data taken on shot
24 - upper probe and shot 25 - upper probe. The corresponding
stress-time curves are also shown. A characteristic of the
foam shots (25 and 26) was a blockage of the polariscope
laser beam. This effect, which is believed to have been
caused by foam material streaming around the back plate and
past the windows of the vacuum chamber, effectively shut off
the polariscope 15 to 20 μsec after arrival of the stress
pulse. Figure 9 indicates this effect. The peak pressures
for the four shots, two probe positions are given in Table II.
The lower probe on shot 25 and the upper probe on shot 26
both registered very small responses that were interfered
with by blockage of the laser beam.

TABLE II

MAXIMUM STRESSES AND APPROXIMATE
STRESS WAVE VELOCITIES OBSERVED
ON SHOTS 23 THROUGH 26

Shot	Probe Position	Maximum Observed Stress In kbar	Approximate Stress Wave Velocity In mm/μsec
23	Upper	2.26	--
	Lower	1.36	--
24	Upper	1.82	2.24
	Lower	0.3	2.56
25	Upper	2.15	2.27
	Lower	--	1.63
26	Upper	--	1.43
	Lower	0.32	--

Stress pulse velocities for the various shots were esti-
mated from the transient time of the stress pulse through the
Plexiglas. The results, which are given in Table II, are only
approximate since they do not take into account time delays
resulting from off-center impacts. The measured velocities
should be compared to the values for velocities of longi-
tudinal and shear waves (c_1 and c_s) in an infinite medium and
the velocity (c_0) of a stress pulse in a finite Plexiglas rod
whose cross-sectional dimensions are less than the wave length
of the principal frequency components of the stress pulse:

$$c_1 = 2.72 \text{ mm/}\mu\text{sec}$$
$$c_s = 1.40 \text{ mm/}\mu\text{sec}$$
$$c_0 = 2.19 \text{ mm/}\mu\text{sec}$$

It appears that near-direct hits produced stress pulses of the
type having velocity close to c_0, while hits which occurred at
larger distances from the stress probes coupled into the probe
as shear waves. The pressure-stress wave velocity data of
M. Van Thiel et al[12] and the observed velocities suggest that
the Plexiglas probes were performing in their elastic region
during shots 23, 24, 25, and 26.

b. Reflection Polariscope Measurements

The behavior of the second plate resulting from impulsive loading by debris impact was studied with the use of the reflection polariscope. The experimental configuration has been described above. Dynamic data were obtained for three impacts. These were for shot numbers 5, 7, and 11, with the material configuration as indicated in Table I above. Selected film strips from these shots are shown, together with photographs of the plate after impact in Figures 10 through 15.

The common feature observed for the three cases is the development and propagation outward of an axisymmetric stress wave consisting of particle motion in the plane of the plate. The wave speed can be determined directly from the distance traveled by a particular fringe and the time between frames. A summary of this data is given in Table III. The time duration for each frame was 1.0×10^{-6} seconds.

TABLE III

REAR PLATE CALCULATED AND

EXPERIMENTAL WAVE SPEEDS

Shot	Material	Measured Wave Speed (mm/μsec)	Calculated * Plate Dilatational Wave Velocity (mm/μsec)	Calculated * Bar Velocity (mm/μsec)
5	Fe	5.27	5.42	5.19
7	Al	5.99	5.41	5.09
11	Fe	4.53	5.42	5.19

* Figures in the columns are calculated from the expression $\sqrt{E/\rho(1-\nu^2)}$ for the dilatational wave velocity, and $\sqrt{E/\rho}$ for the bar velocity together with published values for physical constants.

Frame Number: 1   2   3   4   5   6

7   8   9   10   11   12

13.   14   15   16   17   18

Figure 10.   Shot 5 Response, 3/4 in. Iron Plate, 1.04 µsec
Between Frames.   Lapsed Time From Impact To
First Frame: 1 µsec.

33

Figure 11.   Shot 5 After Impact

Frame Number: 1   2   3   4   5   6

7   8   9   10   11   12

13   14   15   16   17   18

Figure 12.   Shot 7 Response, 3/4 in. Aluminum Plate, 1.06 μsec
             Between Frames.   Lapsed Time From Impact To
             First Frame: 0 μsec.

Figure 13.   Shot 7 After Impact

Frame Number: 1   2   3   4   5   6

7   8   9   10   11   12

13   14   15   16   17   18

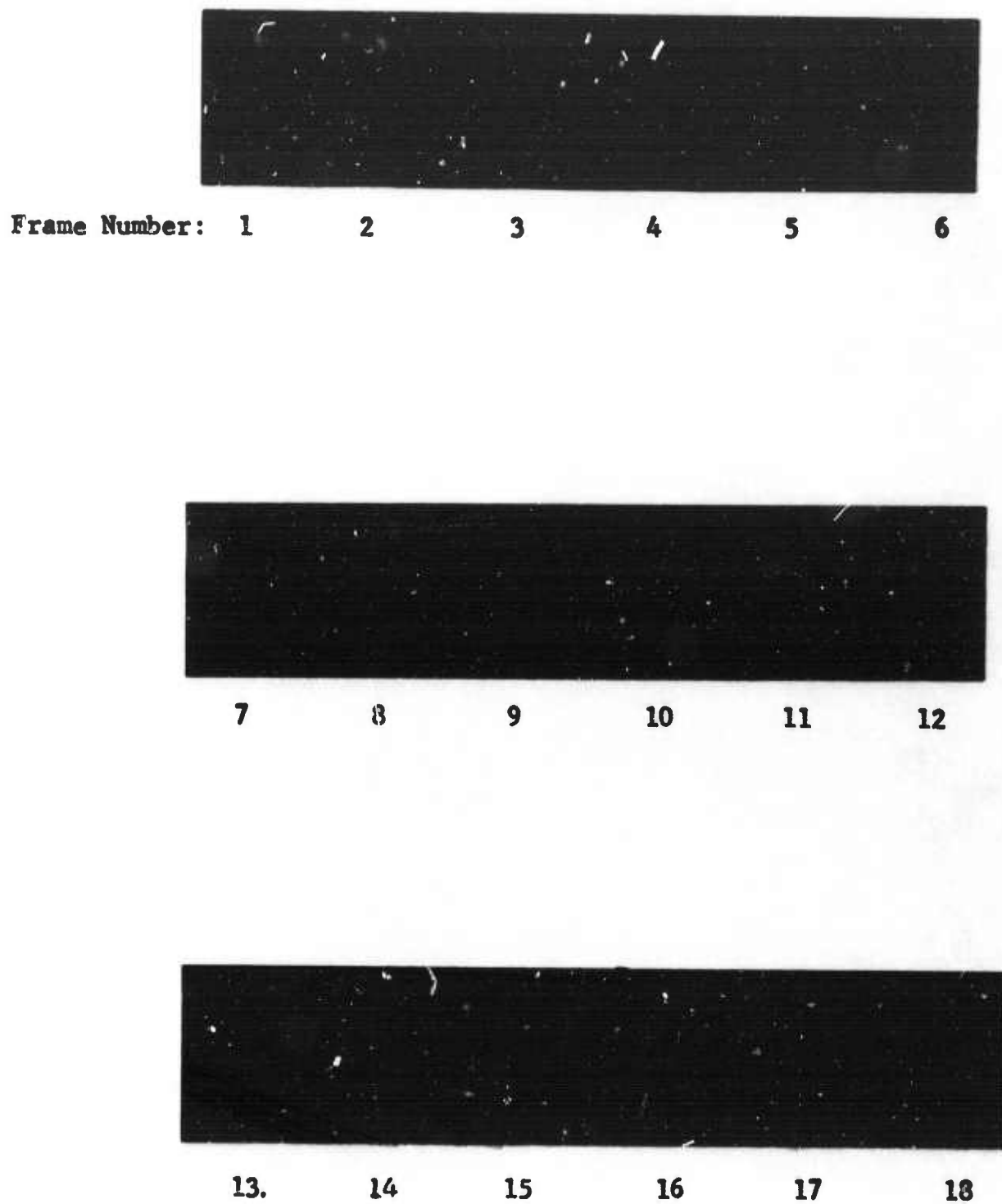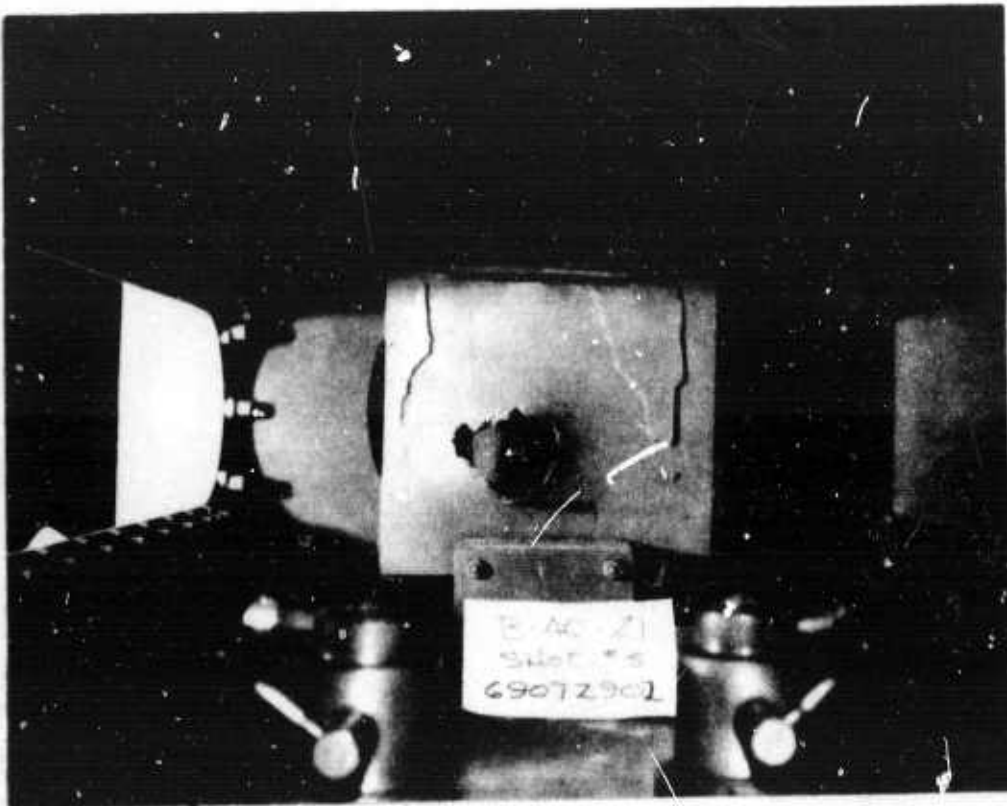Figure 14.   Shot 11 Response, 3/4 in. Iron Plate, 1.05 μsec
             Between Frames.   Lapsed Time From Impact To
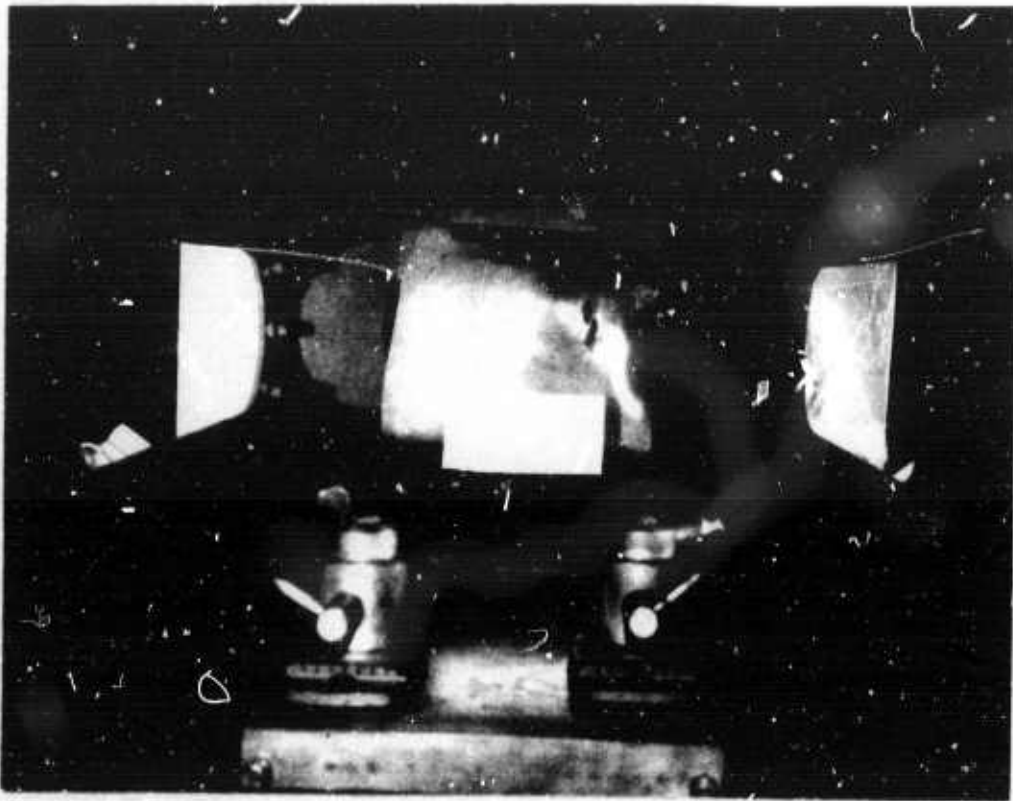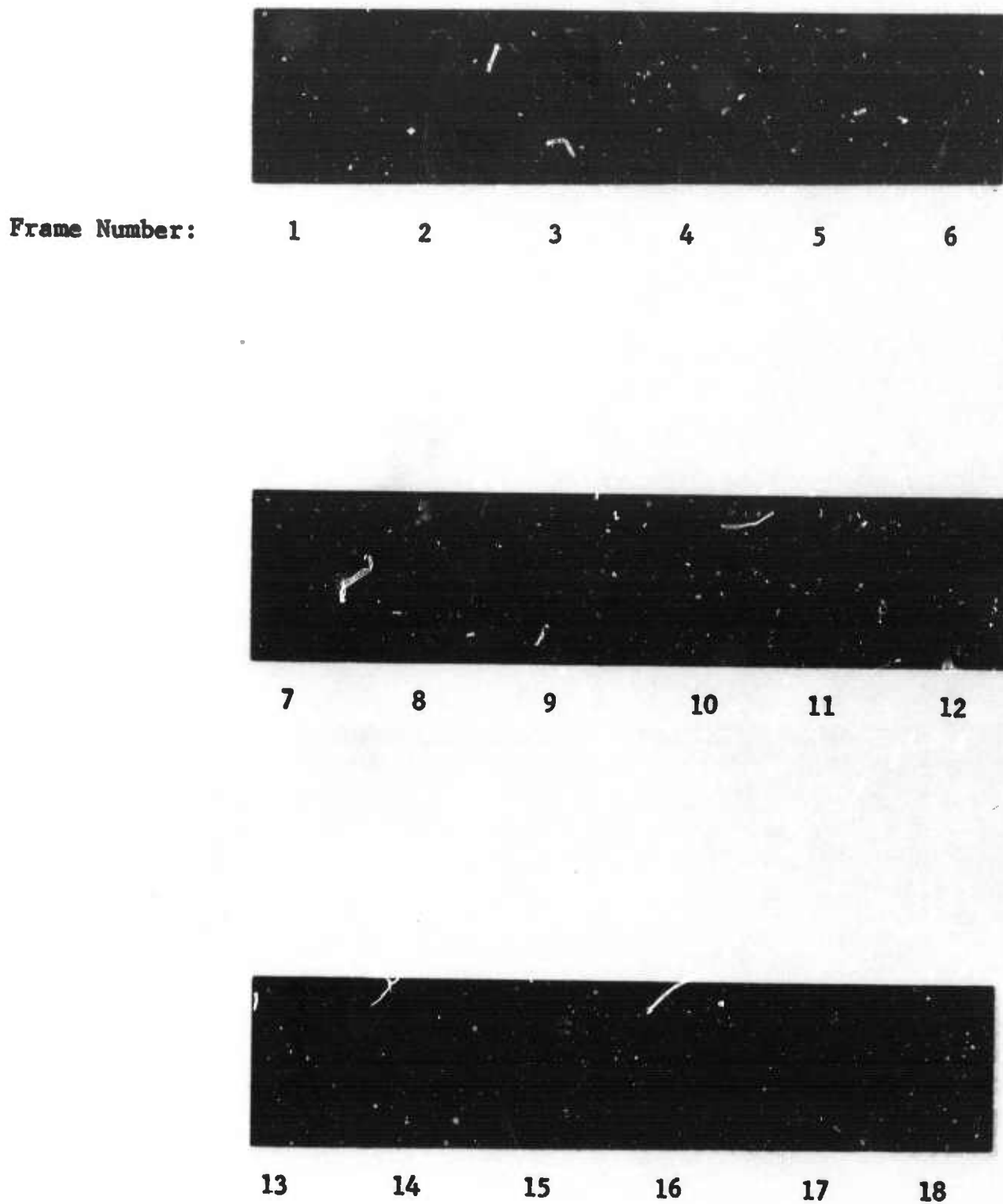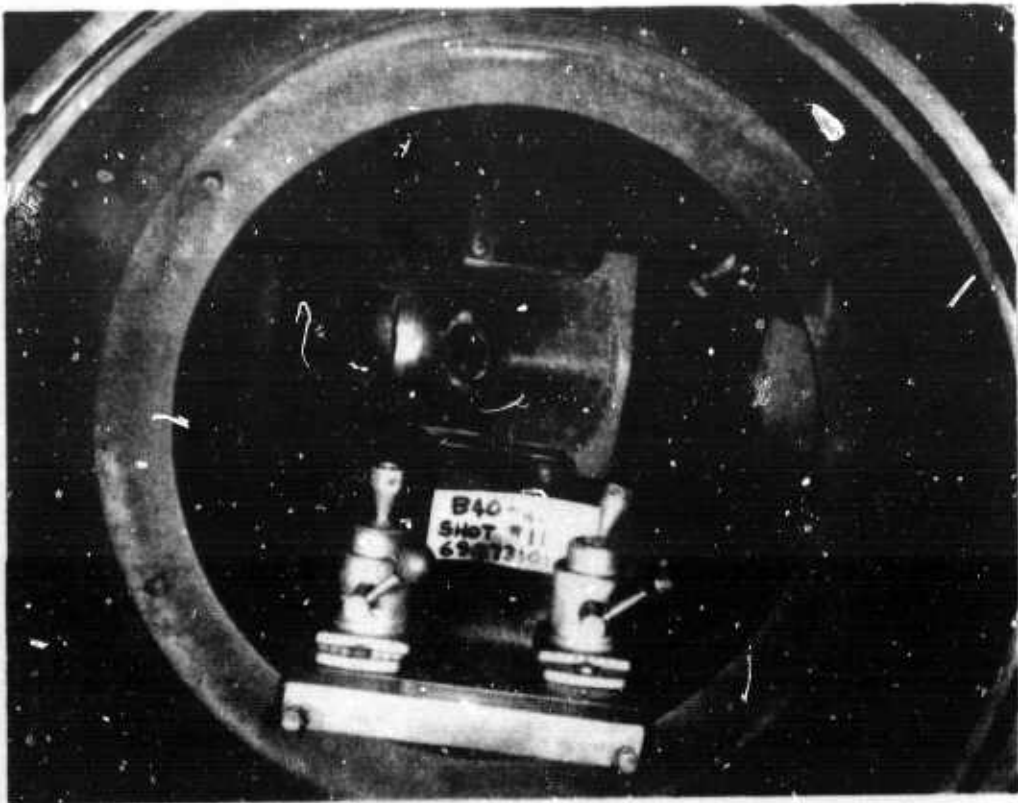   First Frame: 0 μsec.

Figure 15. Shot 11 After Impact

In the case of shot 5, the speed lies between the dilatational plate velocity, $\sqrt{E/\rho(1-\nu^2)}$, and the bar velocity, $\sqrt{E/\rho}$ where E is Young's modulus, ν is Poisson's ratio, and ρ is the density. For shot 11, on the other hand, the speed is somewhat less than either. These results are in agreement with those of Christie[13], who has shown that photoelastic fringes associated with cylindrical dilatational waves are circles and are associated with radial displacements.

Distortional waves on the other hand will travel at about 0.6 the speed of dilatational waves and are associated with circumferential displacements. Fringe patterns in the latter case will lack the axisymmetric form associated with dilatational waves [14]. Examination of the fringe distributions for the case of shots 5 and 11 show this behavior. That is, a cylindrical fringe pattern coming first in time followed by a more complex pattern associated with the development of distortional waves.

Further information may also be obtained with respect to the time history of the loading. The distance across a fringe will be given generally by the product of the duration of the loading and the wave velocity. Closely spaced, narrow fringes as in shot 5, Figure 10, represent, therefore, a rapid loading rate compared to the case of shot 11 in Figure 14.

The wave speed provides some insight into the physical processes that are occurring in the plate. Since it is close to the elastic wave velocity, it indicates that material strength properties are affecting plate response in these regions surrounding the impact point and in the time interval recorded. Additionally, some estimate can be made as to the amplitude of the stress associated with this extensional wave motion. In Figure 14, for example, the out-lying light ring

represents one-half fringe, the next inner dark ring represents a
full fringe and the next light ring represents a fringe and one-
half and possibly another half fringe. For Homalite 100, the
stress for one-half fringe is 32 bars. It can be estimated,
therefore, that the peak of the stress associated with the
extensional wave motion in the coating for this shot is 48
bars for one and one-half fringes. The corresponding stress
in the metal plate is then determined from the expression,

$$\sigma_m = (E_m/E_c) \times \left[(1 + \nu_c)/(1 + \nu_m) \right] \sigma_c \quad (17)$$

where σ_m and σ_c are, respectively, the radial stresses in the
metal and coating, E_m and E_c, respectively, Young's moduli for
the metal and coating, and ν_m and ν_c, respectively, Poisson's
ratios for metal and coating. Clark and Sandford[15] have deter-
mined a value for the dynamic Young's modulus for Homalite 100
of 4.39×10^4 bars. Poisson's ratio for the material is not
given in the manufacturer's data sheet, hence a value of 0.4 is
assumed which is typical of photoelastic materials of this type.
With handbook values for iron, Equation 17 gives a value of 236
bars for the peak stress in the iron.

The response of the aluminum plate is unique in that a large
amount of plastic flow occurred without appreciable rupture. As
seen in Figure 12, the development of the fringes outward occurs
generally as in the case of the steel, but after about six micro-
seconds, the stress begins to develop an interesting structure and
a high loading rate is indicated initially. In later frames,
however, the fringes are becoming "washed out." The reason for
this is not known and does not seem to occur in the case of the
steel plate response. It may perhaps be associated with the
onset of plastic flow or separation of the coating from the plate
leading to the beginning of stress relief.

The experimental results presented above can be related further to a consideration of impact phenomena generally. The subject has been reviewed by Goldsmith[16].

The present case of perforation or extensive plastic deformation of the second plate from debris cloud impact is unique in that the subject usually is concerned with the impact of two solid bodies. The observed results, nevertheless, are in good agreement when considered from the point of view of the response of the impacted body.

Goldsmith considers three principal impact regimes. The first is defined as including stress levels up to roughly an order of magnitude larger than the yield stress. This would be of the order of 10 kbar for aluminum and somewhat more, but of the same or less for steel. In a second or intermediate category, the target will spall, shatter, or be pulverized together with a large attendant dissipation of energy. In the third regime, stresses of the order of the elastic modulus are generated and an analysis based on the methods of hydrodynamics with the materials being considered as compressible fluids, is used in considering penetration phenomena.

An important characteristic of the response of a solid body to impact in the first two categories is the presence of wave phenomena resulting from material elastic and elastic-plastic response. A significant feature of the response is that a major fraction of the energy appearing as wave motion is contained in components of relatively long wave lengths. In addition to wave propagation, target perforation will occur in the case of sufficiently thin targets. Perforation will involve the simultaneous action of a variety of complicated mechanisms, including crack formation and propagation, spallation, dishing, petaling[17], and frictional heating.

The results of the present experiment for second plate response are in good accord with these considerations. Perhaps the most significant result is the presence of measurable elastic wave phenomena, accompanying perforations, from the gaseous debris cloud. The calculation of the minimum wavelength; corresponding to an impact duration of 50 μsec, of the extensional wave motion in the plate leads to a ratio of plate thickness to minimum wave length of about 0.006 and verifies that the head of the wave pulse should travel with the plate extensional speed given by $\left[E/\rho(1-\nu^2) \right]^{1/2}$, as based on dispersion curves for extensional wave motion in a plate[18].

SECTION V

CONCLUSIONS

The present report has been concerned with the application of photoelastic techniques to the problem of hypervelocity impact. Two aspects of the phenomenon have been investigated and demonstrate the practical usefulness of dynamic photoelastic methods in obtaining experimental data. In the first, the pressure time history associated with the stagnation of impact debris on a plate was measured as a photoelastic response in Plexiglas in a new version of the Hopkinson pressure bar technique. For the second, the dynamic response of a second plate to debris impact was studied with a photoelastic coating and a reflection polariscope.

The Plexiglas Hopkinson bar utilized a transmission polariscope with a helium-neon laser serving as a source of monochromatic, polarized light. The pressure-time history of debris impact was determined by recording the transient change in light level produced during passage of the stress wave. An analysis of dispersive effects indicated that these did not significantly affect the results.

The reflection polariscope recorded a whole field view of the dynamic response of aluminum and steel plates. The method utilized a high-speed framing camera and provided a continuous record of the extensional wave motion in the plate in the range to roughly 50 μsec after impact.

The plate response made evident the range of phenomena that can be expected to occur as a result of debris impact and that should be taken into account in describing the phenomena theoretically. First, measurable elastic phenomena reflecting material strength, occur in the impacted plates and in the time regime noted and accompany the plastic flow and destructive aspects of the impact. Second, the presence of wave phenomena can lead to the formation of stress concentrations due to wave interaction and to failure modes characteristic of the early elastic regime that might

not be evident if the phenomena is described in the context of a purely
hydrodynamic or rigid-plastic theoretical approach. Lastly, the experi-
mental methods, investigated in preliminary form in this study, can also
yield information on the dynamic values of the physical constants involved
that will prove useful in correlative computer studies of impact phenomena.

REFERENCES

1. Hopkinson, B., Phil. Trans. A213, 437 (1914).

2. Davies, R. M., Phil. Trans. A240, 375 (1948).

3. Morse, R. W., Journ. Acoust. Soc. Amer. 22, 219 (1950).

4. Kolsky, H., Phil.Mag. 8, 693 (1956).

5. Kolsky, H., Stress Waves in Solids, Dover Publications, Inc. New York, 1963, p. 99.

6. Hunter, S. C., Mechanics and Chemistry of Solid Propellants, Ed. Eringen, Liebowitz, Koh, Crowley, Pergamon Press, London, 1967, p. 257.

7. Hendry, A. W., Photoelastic Analysis, Pergamon Press, Inc., New York, 1966, and the references contained therein.

8. Durelli, A. J., Riley, W. F., Introduction to Photomechanics, Prentice-Hall, Inc., Englewood Cliffs, New Jersey, 1965.

9. Dally, J. W., and Riley, W. F., Experimental Stress Analysis, McGraw-Hill, Inc., New York, 1965.

10. Cole, C. A., Jr., Quinlan, J. F., and Zandman, F., Proc 5th International Congress on High-Speed Photography, J. Soc. Motion Picture and Television Engineers, 1962, p. 252.

11. Flynn, J., Soc. Motion Picture and Television Engineers 75, 729 (1966).

12. Van Thiel, M., Kusulow, A. S., and Mitchell, A. C., Compendium of Shock Wave Data, UCRL-50108, Vol. 2, Suppl. 1, Lawrence Radiation Laboratory, October 1967.

13. Christie, D. G., Phil. Mag., 46, 527 (1955).

14. Dally, J. W., Durelli, A. J., Riley, W. F., Proc. of the Soc. for Exp. Stress Analysis, 17, 33 (1960).

15. Clark, A. B. J., Sanford, R. J., Exp. Mech. 3, 148 (1963).

16. Goldsmith, E., App. Mech. Revs. 16, 855 (1963).

17. Goldsmith, W.; Liu, T. W.; Chulay, S., Exp. Mech., Dec. 1965, p. 385.

18. Kolsky, H., Stress Waves in Solids, Dover Publications, Inc., New York, 1963, p. 79.

DOCUMENT CONTROL DATA - R & D

(Security classification of title, body of abstract and indexing annotation must be entered when the overall report is classified)

1. ORIGINATING ACTIVITY *(Corporate author)*	2a. REPORT SECURITY CLASSIFICATION
Hughes Aircraft Company Fullerton, California 92634	UNCLASSIFIED
	2b. GROUP

3. REPORT TITLE

INVESTIGATION OF DYNAMIC MECHANICAL STRESS WITH PHOTOELASTIC TECHNIQUES

4. DESCRIPTIVE NOTES *(Type of report and inclusive dates)*
1 April 1969 through 3 September 1969

5. AUTHOR(S) *(First name, middle initial, last name)*

V. R. Honnold; C. C. Berggren; W. M. Peffley

6. REPORT DATE	7a. TOTAL NO. OF PAGES	7b. NO. OF REFS
April 1970	52	18

8a. CONTRACT OR GRANT NO.	9a. ORIGINATOR'S REPORT NUMBER(S)
F29601-69-C-0095 *new*	
b. PROJECT NO.	AFWL-TR-69-154
0251	
c.	9b. OTHER REPORT NO(S) *(Any other numbers that may be assigned this report)*
d.	

10. DISTRIBUTION STATEMENT   This document is subject to special export controls and each transmittal to foreign governments or foreign nationals may be made only with prior approval of AFWL (WLTA), Kirtland AFB, NM. Distribution is limited because of the technology discussed in the report.

11. SUPPLEMENTARY NOTES	12. SPONSORING MILITARY ACTIVITY
	AFWL (WLTA) Kirtland AFB, NM 87117

13. ABSTRACT   (Distribution Limitation Statement No. 2)

The technique of dynamic photoelasticity has been applied to a study of hypervelocity impact phenomena. The target consisted of a cadmium front plate, followed either by a void or a foam filled space, and a rear plate of steel or aluminum. Two series of tests were carried out. The first, employing a Plexiglas rod, acting as a Hopkinson pressure bar in a transmission polariscope arrangement, sensed the pressure time history resulting from debris stagnation in the second plate. In the second series, the rear plate was provided with a photoelastic coating as part of a reflection polariscope. Dynamic stress patterns, produced by a debris impact, were photographed as they developed in time and provided a whole field view of the nature of the pattern. The experimental results indicate that Plexiglas can be used successfully as a pressure bar for dynamic stress measurements in the range of several kilobars. Analysis of dynamic plate motion indicates the presence of elastic extensional waves and shows that second plate deformation and rupture are accompanied by elastic effects.

PRECEDING PAGE BLANK

DD FORM 1473
1 NOV 65

14. KEY WORDS	LINK A		LINK B		LINK C	
	ROLE	WT	ROLE	WT	ROLE	WT
Birefringence						
Dynamic stress birefringence						
Stress coating						
Dynamic pressure measurements						
Hypervelocity impact						
Hopkinson pressure bar						
Photoelastic coating						
Target Plates						
Photoelastic Theory						
Stress-wave propagation						